HYDROLOGICAL PROCESSES
Hydrol. Process. **30**, 2835–2850 (2016)
Published online 13 April 2016 in Wiley Online Library
(wileyonlinelibrary.com) DOI: 10.1002/hyp.10817

Modeling the sediment yield and the impact of vegetated filters using an event-based soil erosion model—a case study of a small Canadian watershed

Gabriel Hould-Gosselin,[1] Alain N. Rousseau,[1]* Silvio J. Gumiere,[2] Dennis W. Hallema,[2] Claudie Ratté-Fortin,[1] Georges Thériault[3] and Eric van Bochove[3]

[1] *INRS–ETE, 490 rue de la Couronne, Québec, Québec, G1K 9A9, Canada*
[2] *Université Laval, Département des Sols et de Génie Agroalimentaire, 2480 boulevard Hochelaga, Québec, Québec, G1V 0A6, Canada*
[3] *Agriculture and Agri-Food Canada, Soils and Crops Research and Development Centre, Science and Technology Branch, 2560 Hochelaga Blvd, Québec, Québec, G1V 2J3, Canada*

Abstract:

This paper presents the first application of the event-based MHYDAS-Erosion model to a small agricultural watershed under temperate climate conditions (Quebec, Canada). Simulation results based on observed and synthetic rainfall events revealed a bimodal behaviour of sediment yield. During high-intensity rainfall events, most of the sediments reaching the watershed outlet originate from cropland. Meanwhile, during low-intensity events, most of the sediments come from the drainage network. Furthermore, simulation results show that implementation of 5-m and 20-m wide vegetated filters throughout the watershed or at the edge of the most problematic fields (4% of the total fields) could reduce soil loss by 52% and 31%, respectively. The modeling framework could be used for the design and location of beneficial management practices such as grass strips and riparian zones Copyright © 2016 John Wiley & Sons, Ltd.

KEY WORDS hydrologic models; agriculture; soil erosion; case studies

Received 19 June 2015; Accepted 4 February 2016

INTRODUCTION

Intensive agriculture has been identified as one of the major causes of accelerated soil erosion with ablation rates many times higher than those of soil-forming processes. Soil degradation has been observed in many regions of the world, some of them being more prone to erosion than others depending on soil type, topography, vegetation, rainfall intensity and frequency, and agricultural practices. Beneficial management practices (BMPs) such as vegetated filters, terraces and small dams (Callow and Smettem, 2009) that retain water and trap sediment particles have been implemented in sensitive watersheds to break the sedimentological connectivity, that is, the hydrological pathways of agricultural soil and water contaminants (e.g. Quilbé *et al*., 2008; Rousseau *et al*., 2013; Gumiere *et al*., 2014).

Several process-oriented and physically based erosion and hydrological models have been developed to assess soil and water conservation BMPs for watershed managers, planners and policy-makers. The Chemical Runoff and Erosion from Agricultural Management Systems (CREAMS) model (Knisel, 1980), the Kinematic Erosion Simulation model (KINEROS) (Woolhiser *et al*., 1990), the Soil and Water Assessment Tool (SWAT) (Neitsch *et al*., 2011), the Limburg Soil Erosion Model (LISEM) (De Roo *et al*., 1996), the Water Erosion Prediction Project (WEPP) (Ascough *et al*., 1997), the European Soil Erosion Model (EUROSEM) (Morgan and Quinton, 1998) and GIBSI (Rousseau *et al*., 2005, Rousseau *et al*., 2013), to name a few, have been used to estimate overland soil erosion rates and in-stream sediment concentrations at the plot, field and watershed scales. These models are mostly raster-based and not ideal for accurately representing flow paths even with a high-resolution gridded data.

Jetten *et al*. (1999, 2003) suggested that accounting for the temporal variability in precipitation intensities is paramount to adequately simulate dynamic phenomena such as soil erosion and sedimentological connectivity. For example, rainfall can modify the soil structure and induce crusting, changing the surface roughness and water infiltration during an event. Gumiere *et al*. (2011) noted that to mimic the sedimentological connectivity

*Correspondence to: Alain N. Rousseau, INRS–ETE, 490 rue de la Couronne, Québec (Québec) GIK 9A9, Canada.
E-mail: Alain.Rousseau@ete.inrs.ca

some modeling approaches often use an implicit parameter known as the sediment delivery ratio (SDR) (e.g. Agricultural Non-Point Source Pollution Model (AGNPS) (Young and Onstad, 1989); the Guelph model to evaluate the effects of Agricultural Management Systems on Erosion, Sedimentation, and Phosphorus yield (GAMESP) (Rousseau *et al*., 1987, 1988) or a 'black box' method (Bracken and Croke, 2007)). Hence, these approaches cannot provide a real understanding of the spatial and temporal patterns of sediment sources and sinks in a watershed.

Given that soil erosion mostly occurs under high-intensity rainfall, Gumiere *et al*. (2010, 2014) proposed MHYDAS-Erosion, an event-based distributed model for small watersheds (a few km^2), which was adapted to simulate the distributed impact of various BMPs on sedimentological connectivity. The model was implemented and tested in a densely instrumented Mediterranean watershed (Roujan, OMERE Observatory, in southern France) to assess vegetated filters using water and sediment discharge measurements at three nested scales. Discharge and soil loss agreed well with field observations in this watershed; however, to date the model had not been applied under temperate climate conditions.

The main objectives of this study were to: (i) assess the ability of MHYDAS-Erosion to simulate soil loss and sediment transport in an intensively farmed, 2.5-km^2 watershed in southern Québec, Canada, under temperate climate conditions; and (ii) evaluate, using observed and synthetic rainfall events, how different spatial configurations of vegetated filters at the downstream end of the fields can alter the sedimentological connectivity, and thus sediment fluxes, throughout the watershed.

The first part of the paper describes the modeling approach, including spatial representation, topology and equations for flow, soil erosion and sedimentation within the vegetated filters. The last part of the paper presents a case study using MHYDAS-Erosion to the study watershed including model validation and application to study the impacts of vegetated filters on sediment yield.

MODELING OVERVIEW

Spatial discretization and topology

Under the MHYDAS-Erosion modeling framework, a watershed is subdivided into two types of elementary hydrological units, as described in detail by Moussa *et al*. (2002), namely surface units (SUs) and reach segments (RSs) that define the drainage network (Lagacherie *et al*., 2010). For this study, PHYSITEL (Rousseau *et al*., 2011), a discretization tool for distributed hydrological models, was used to determine the drainage network and subdivide the watershed into SUs (i.e. hillslopes) and RSs. SUs were created by intersecting spatial data (Figure 1) such as topography (i.e. 1-m digital elevation model (DEM) derived from LIDAR data), drainage networks (i.e. digitized river network derived from LIDAR data), field boundaries, roads, soil types and BMPs. Each surface unit is connected to one downstream unit, either a SU or a RS. Using this watershed discretization framework, water and sediments can be

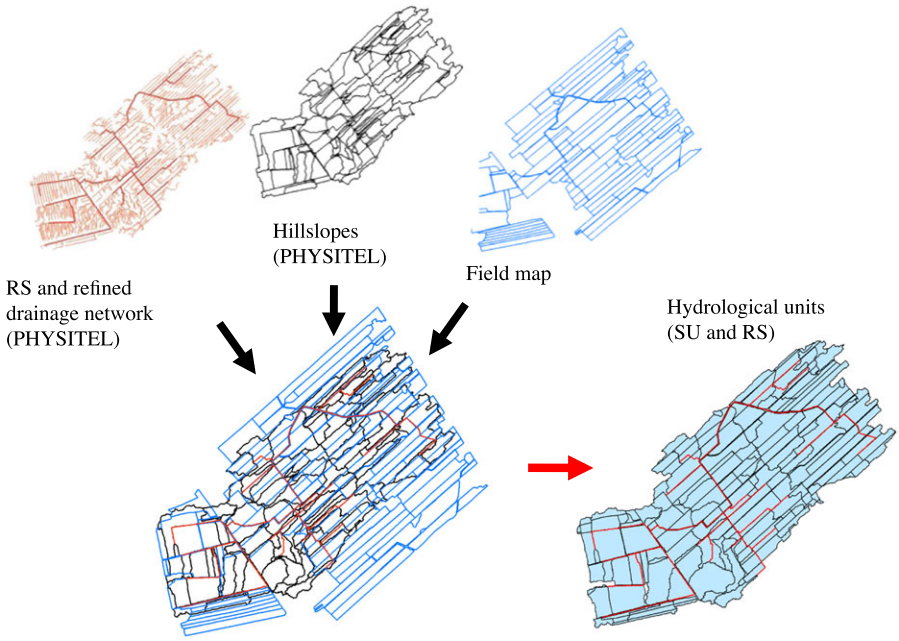

Figure 1. Spatial discretization into surface units (SUs) and reach segments (RSs) using PHYSITEL

tracked from the upper zones of the watershed because SUs are numbered and water and sediment discharge are calculated fallowing a topological process described in Gumiere *et al*. (2010).

Topological links between SU-SU, SU-RS and RS-RS were established from the discretized watershed. Using *in situ* observations, adjustments were made to include hydrological short circuits that cannot be identified by PHYSITEL alone. Short circuits typically included anthropogenic modifications inducing faster surface runoff evacuation toward drainage ditches or preventing water ponding in field depressions. For example, a small culvert under a farm road allows one field to drain into another. Because a farm road is often higher than the surrounding fields, this hydrological connection is not identifiable with the pathways derived by topography alone. Further subdivisions of SUs into 'rill' and 'interrill' units were made to better simulate the sediment transport and soil erosion processes on either type of surface (caused by both runoff and rainfall detachment processes), as shown in Figure 2. The subdivision consisted in linearizing both rill and interrill areas according to the SU shape and slope parameters. The number of rills for each SU is dependent on land cover, *in situ* observations, and can be naturally occurring or induced by anthropogenic influences (see next section, third paragraph). In order to ensure model stability, the number-of-rills (N_{Rill}) parameter range should be set between 1 and 30. MHYDAS-Erosion was developed initially for vineyards where rills for concentrated flows are easily identified. For this study, N_{Rill} was fixed to 30 indicating a more diffuse behaviour because land cover throughout the watershed for the simulation period was mostly corn (*Zea mays*, 20%), oats (*Avena sativa*, 6%) and soy (*Glycine max*, 31%). This parameter has a strong influence on sediment exports from SUs and consequently on the vegetated buffer efficiency.

Hydrological and soil erosion processes

Rainfall events are divided into t time steps of length Δt, for which the hydrological and soil erosion equations are solved independently, but successively within the same time step, using a backward explicit finite difference scheme. Figure 3 illustrates the interdependencies of the processes involved during one time step for one hydrological unit (SU or RS).

At a given time step t for a hydrological unit i, the hydrological variables q_i^t, v_i^t and h_i^t (i.e. unit flow discharge, flow velocity and water height, respectively) are calculated using the hydrological module of MHYDAS. To ensure model stability according to the Courant Friedrichs Lewy (CFL) condition (Courant *et al*., 1928), time steps are short enough to correctly simulate the highest possible flow velocities. Rainfall is partitioned on SUs between runoff and infiltration based on rain characteristics, initial soil water content and saturated hydraulic conductivity according to the analytical solution developed by Moussa (1996). Infiltrated water is assumed to flow vertically through an unsaturated layer where it can flow to groundwater.

The excess rainfall for each unit is converted into a surface runoff hydrograph routed to the outlet of the hydrological unit using the analytical solution of the Hayami model for the one-dimensional Saint-Venant equation (Hayami, 1951; Moussa *et al*.,1996). Hydrolog-

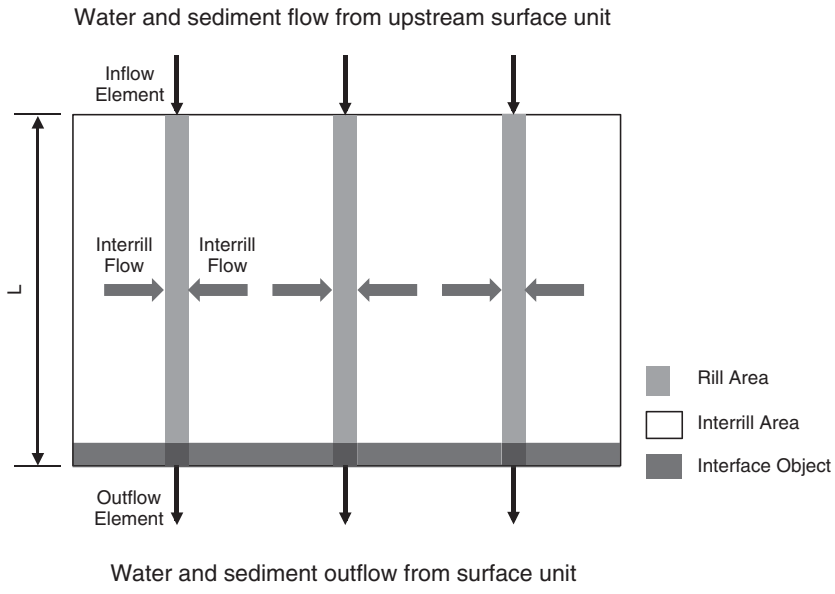

Figure 2. Spatial topology and separation of a SU into rills and interrills (adapted from Gumiere *et al*., 2010)

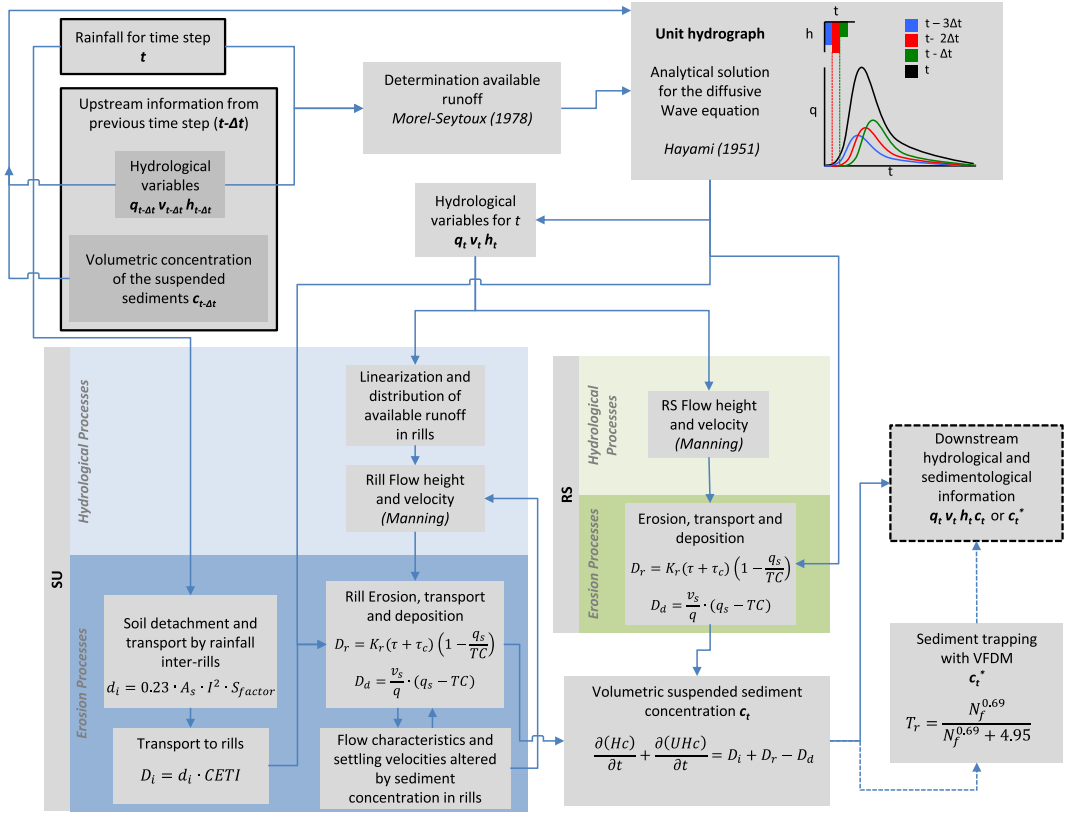

Figure 3. Interdependencies of processes during one time step on one hydrological unit (SU or RS), where h (m) is flow height, v ($m\,s^{-1}$) is flow velocity, t (s) is current time step and c ($kg\,m^{-3}$) is sediment concentration. The outlined boxes show the hydrological and sedimentological variables required as inputs for the current time step (t), and the dashed box shows the resulting hydrological and sedimentological variables after time step (t) at the downstream end of the current hydrological unit

ical information for time step $t - \Delta t$ from both the upstream discharge and the current hydrological unit are used to find the solution. The flow depth and velocity within the linear RSs and within the rill partitions of the SUs are then obtained with the Manning formula using either the observed or calculated slope, shape and width of each SU. The flow height within the SU rills depends on the number of rills specified, as the available runoff is distributed equally for all of the rills of one SU.

Once the flow characteristics calculated, the erosion equations are solved. The erosion module is based on the mass conservation equation applied to the sediment load as proposed by (Bennett, 1974):

$$\frac{\partial(Hc)}{\partial t} + \frac{\partial(UHc)}{\partial x} = D_i + D_r - D_d \tag{1}$$

where H (m) is the flow height and U ($m\,s^{-1}$) the mean flow velocity within the rills or RSs, t (s) time, c ($kg\,m^{-3}$) the sediment concentration, D_i ($kg\,m^{-2}\,s^{-1}$) the sediment inflow rate from interrill erosion, D_r ($kg\,m^{-2}\,s^{-1}$) the sediment inflow rate because of rill erosion and D_d ($kg\,m^{-2}\,s^{-1}$) the sediment deposition rate in the rills. At the SU level, D_i and D_r are designed to take into account erosion caused both by runoff and rainfall detachment. The erosion module assumes that all particles travel at the mean velocity. Furthermore, only suspended sediment transport is simulated; bedload particle transport by sliding and rolling is ignored. Erosion, transport and deposition in RSs are calculated using the same method as that used for the rills, and the flow characteristics provided by the Manning formula is adapted to the channel dimensions.

Erosion and transport processes in rill and interrill areas on SUs are thus influenced by three driving sources of energy. As conceptualized by Kinnell (2005), energy dissipated by raindrops and raindrop-induced flow represent the driving variables for soil detachment and transport between rills and surface flow detachment caused by runoff.

As illustrated in Figure 3, the transport and erosion equations for rill and interrill areas are solved in a sequence. The sediment inflow rate from interrill erosion D_i depends only on the rainfall intensity at the current time step. The equation for these processes is as follows:

$$D_i = 0.23 \cdot A_s \cdot I^2 \cdot S_{factor} \cdot CETI \tag{2}$$

where A_s is the index of stability (Yan *et al*., 2008; Shi *et al*., 2010), I ($\mathrm{mm\,h^{-1}}$) the rainfall intensity, S_{factor} ($\mathrm{m\,m^{-1}}$) the slope factor calculated by $1.05-0.85\cdot e^{-4sin\theta}$ and θ the slope angle, and CETI the efficiency of transport in interrills (—). The index of stability, A_s, is based on Zhang and Horn (2001):

$$A_s = \frac{MWD_{SW} - MWD_{FW}}{MWD_{SW}} \cdot \frac{MWD_{SW} - MWD_{WS}}{MWD_{SW}} \tag{3}$$

where MWD_{SW} (m) is the mean weight diameter obtained by slow-wetting treatment, MWD_{FW} (m) the mean weight diameter obtained by fast-wetting treatment and MWD_{WS} (m) the mean weight diameter obtained by stirring treatment.

As surface flow heights are rarely considered to be high enough to use conventional flow equations, the concept of efficiency of transport in interrills (CETI) was introduced to describe the effect of surface roughness on the interrill-to-rill erosion runoff contribution. The *CETI* values are calculated as follows:

$$CETI = CETI_{max}\cdot\left(1 - e^{\alpha\cdot R}\right) \tag{4}$$

where $CETI_{max}$ (—) is the maximum allowed value of *CETI*, α (—) an empirical exponent that depends on roughness and R ($\mathrm{mm\,h^{-1}}$) the runoff amount.

The sediment inflow rates because of rill erosion, D_r, integrate aspects of the particle detachment because of excess shear stress when the transport capacity of the flow exceeds the current sediment load and sediment transport caused by runoff in the SU. The equation proposed by Foster *et al*. (1995) is used to determine D_r:

$$D_r = K_r(\tau - \tau_c)\left(1 - \frac{q_s}{TC}\right) \tag{5}$$

where K_r ($\mathrm{s\,m^{-1}}$) is the rill erodibility; τ (Pa) the shear stress exerted on the bed by the flow; τ_c (Pa) the critical shear stress over which detachment is initiated; q_s ($\mathrm{kg\,m^{-1}\ s^{-1}}$) the unit solid discharge by a 1-m width of the flow calculated as $q_s = q\cdot c$, where q is the unit flow discharge per meter width of the flow ($\mathrm{m^2\,s^{-1}}$); and *TC* ($\mathrm{kg\,m^{-1}\ s^{-1}}$) the transport capacity, which measures the ability of the flow to carry a sediment load, and it is empirically related to the values of τ and τ_c, as follows (Foster, 1982):

$$TC = \eta\cdot(\tau - \tau_c)^k \tag{6}$$

where η ($\mathrm{m^{1/2}\ s^2\ kg^{-1/2}}$) is the efficiency of the transport with the recommended values of η and k (0.04 and 1.5, respectively) according to the study of Finkner *et al*. (1989). *TC* depends on both the suspended sediment flux given by the Hayami function and the influx of sediments from interrill areas during the same time step, as illustrated in Figure 3.

The sediment deposition D_d is calculated when $q_s > TC$ (Foster *et al*., 1995):

$$D_d = \frac{v_s}{q}\cdot(q_s - TC) \tag{7}$$

where v_s ($\mathrm{m\,s^{-1}}$) is the settling velocity, which is calculated with the equation proposed by Soulsby (1997):

$$v_s = \frac{v}{d_s}\cdot\left[\sqrt{10.36^2 + 1.049\cdot(1 - c_{vol})^{4.7}\cdot d_{s*}^3} - 10.36\right] \tag{8}$$

where v ($\mathrm{m^2\,s^{-1}}$) is the kinematic viscosity of water, d_s (m) is the diameter of the flow particles, c_{vol} (—) the volumetric concentration of particles and d_{s*} (—) the dimension less sedimentological diameter, calculated by:

$$d_{s*} = d_s\left[\frac{(\rho_s/\rho)\cdot g}{v^2}\right]^{1/3} - 1 \tag{9}$$

where ρ_s and ρ ($\mathrm{kg\,m^{-3}}$) are the densities of particles and water, respectively.

Modeling vegetated filters (coupling MHYDAS-Erosion and VFDM)

The computational units of MHYDAS-Erosion are generally smaller than fields and thus allow for the integration of spatially distributed sediment-trapping BMPs at the intersection of any topologically linked hydrological units (SU-SU and SU-RS). Thus, the coupling of MHYDAS-Erosion with VFDM, the Vegetated Filter Dimensioning Model of Gumiere *et al*. (2013) (see also Gumiere *et al*., 2015), provides a way to simulate sediment trapping by vegetated filter strips at the downstream end of chosen SUs. As observed in Figure 3, for the chosen SUs, VFDM uses outputs from MHYDAS-Erosion (i.e. flow rates and volumetric sediment concentrations at every time step) to simulate sediment abatement. Strips are modelled as a vegetated barrier that runs the total length of the connecting hydrological units, which offers a barrier that is orthogonal to the mean flow velocities. The vegetated filter behaviour is derived from the flume experiments conducted by Deletic (2005) and Deletic and Fletcher (2006); and the sediment-trapping efficiency T_r is calculated with the following equation:

$$T_r = \frac{\left(\frac{l\cdot V_s}{h\cdot V}\right)^{0.69}}{\left(\frac{l\cdot V_s}{h\cdot V}\right)^{0.69} + 4.95} \tag{10}$$

where l (m) is the grass strip width, h (m) depth of flow over vegetation, V_s (m s^{-1}) the Stokes settling velocity for the sediment particles and V the mean flow velocity between the grass blades (m s^{-1}). Once Equation 10 is solved for one time step, the module calculates the altered sediment concentrated values, c_i^*, available to the downstream unit and feeds the next time step using the following equation:

$$c_i^* = c_i(1 - T_r)\ . \tag{11}$$

All hydrological and erosion variables used by VFDM are calculated by MHYDAS-Erosion.

Conversely, VFDM can also solve Equation 11 to provide the required vegetated filter width (l) at every time step to obtain a predefined trapping efficiency. Therefore, two outputs for each SU are generated; namely: (i) the sediment abatement efficiencies per time step calculated for a predefined filter width; and (ii) vegetated filter widths determined at every time step to obtain a predefined trapping efficiency.

The relative vegetation density (grass) in the strips is set to a value of 0.6 (on a scale between 0 and 1), as suggested by Gumiere *et al.* (2013) for the greater Beaurivage watershed, which includes the current experimental watershed. VFDM was chosen here because of its simple parameterization when compared to other models such as VFSMOD (Munoz-Carpena *et al.*, 1999; Akram *et al.*, 2015), which are often difficult to parameterize at large and distributed scales. Because of the current coupling of VFDM with MHYDAS-Erosion, the performance of the sediment trapping intrinsically depends on the quality of the simulated overland flow. It is noteworthy that in its current version the event-based MHYDAS-Erosion model does neither simulate snow processes (i.e. accumulation and melt) nor erosion processes under spring conditions.

MATERIAL AND METHODS

Study site

This study was conducted on an experimental micro-watershed (2.4 km^2) located in the Bras d'Henri River (150 km^2) watershed, which is part of the Chaudière watershed, Quebec, Canada (see Figure 4). Annual precipitation averages 1100 mm. The Bras d'Henri is intensively farmed with an animal density of 4.7 animal units per hectare of farmland, which highlights the importance of livestock production in the area. The micro-watershed has similar characteristics: it is intensively farmed (84% of the watershed) and has very few wooded areas (mainly located in the southwest portion of the watershed) that cover 13% of the total area. The remaining 3% of the land is built up. Two main waterways comprise the drainage network (branches 14 and 15) and converge at the outlet. In 2012, the cropland in the micro-watershed was mainly used for corn (*Z. mays*, 20%), oats (*A. sativa*, 6%), soy (*G. max*, 31%) and

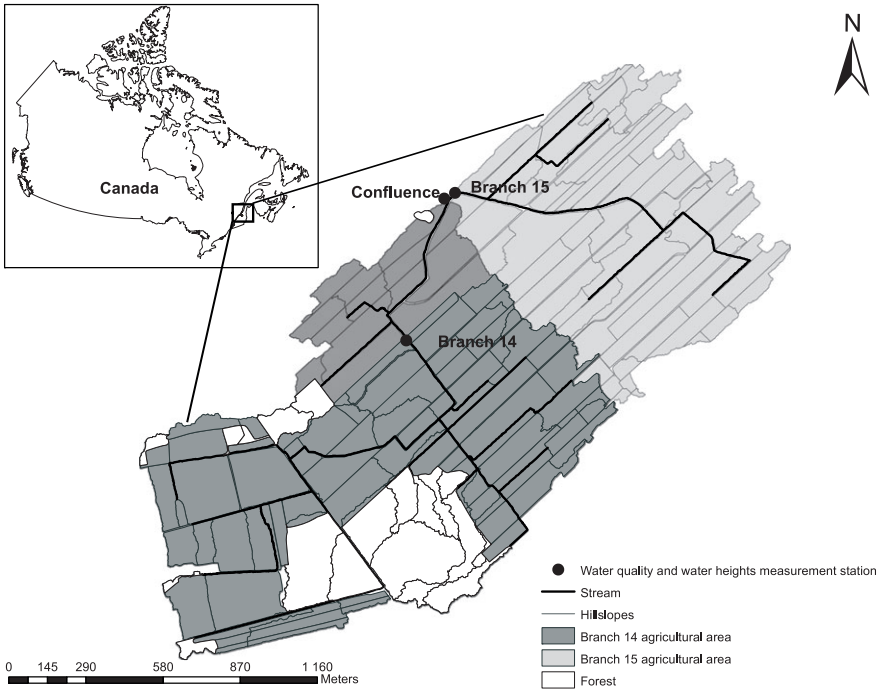

Figure 4. Experimental Bras d'Henri micro-watershed, Quebec, Canada

prairies (24%). A large proportion of soy (*G. max*) was farmed with residues left from the previous growing seasons (58% with residue, 42% without), and 3% of the prairies were sowed late, which exposed bare soils over a longer period when compared to the other cultures. Figure 5 also shows the final SU and RS map for the Bras d'Henri micro-watershed and the spatial distribution of land cover.

The soil types are mainly loamy sands and sandy loams which generally have a low critical soil shear stress and are highly erodible. They are also the least suitable for the purpose of agriculture because of leaching of nutrients and limited water holding capacity, and as a result, these source areas for sediments are mostly used for livestock farming. Table I shows the different types of soils and their properties, as identified by a soil survey conducted in 2009 by Agriculture and Agri-Food Canada (AAFC) (Lamontagne *et al.*, 2010). Approximately 30% of the watershed is tile-drained (AAFC Agriculture and Agroalimentaire Canada, 2013).

Table I. Soil characteristics in the Bras d'Henri watershed

Soil type	Area (%)
Mineral soils	86.2
Loams	*56.1*
Sands	*26.7*
Skeletal	*3.4*
Organic soils	11.2
Unclassified	2.6
Total	100

Rainfall events

Table II shows the characteristics of the eight rainfall–runoff events that were recorded during the 2012 field campaign. Note that in the table, NAPI refers to the Normalized Antecedent Precipitation Index of Heggen (2001). Summer events are more akin to convective events in terms of their intensities, unlike autumn events. The 5th and 10th of August and the 19th of October events (in bold) were the most likely to have produced soil

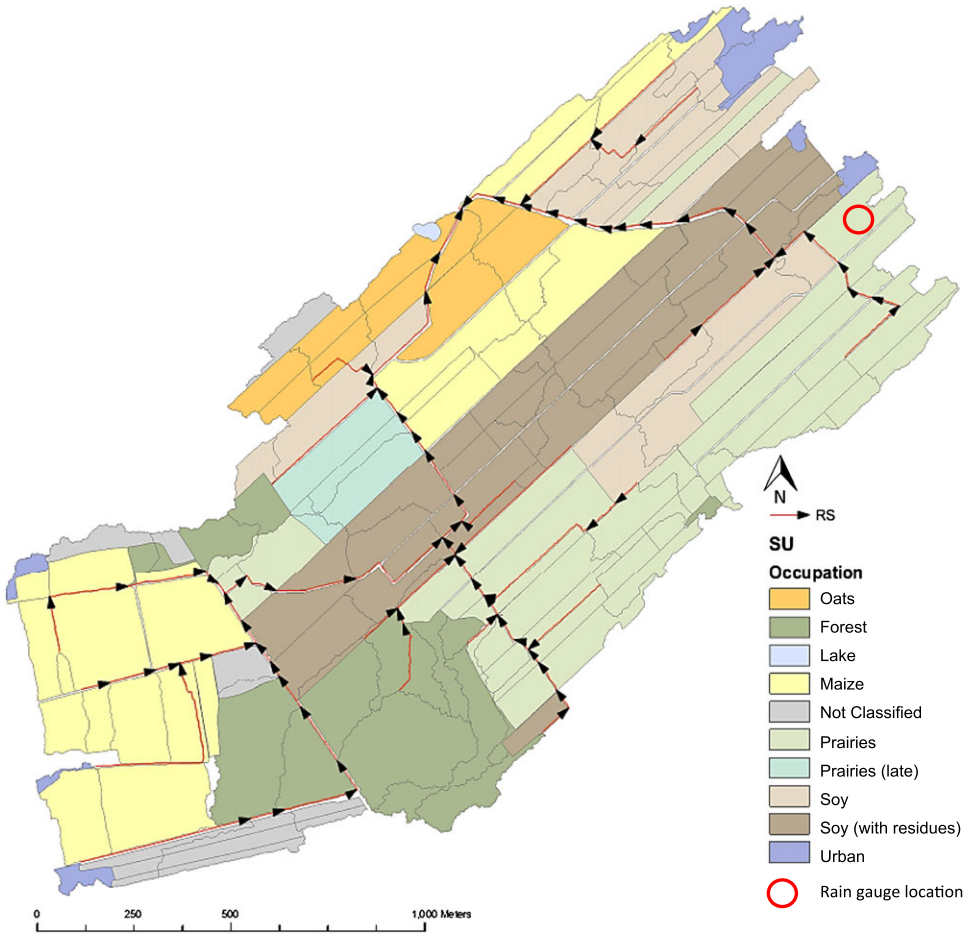

Figure 5. Map of hydrological units (SUs and RSs) and land cover. The gray lines represent SU boundaries; the red lines represent linear RSs (arrow heads illustrate the flow direction)

Table II. Rainfall characteristics of the 2012 events used in the calibration of MHYDAS-Erosion

Date	Duration (h)	Total precip. (mm)	Mean intensity ($mm\,h^{-1}$)	Max. intensity ($mm\,h^{-1}$)	NAPI 5	NAPI 2	Peak flow rate (l/s)
2012 Jul. 04	8	14.4	1.81	11.9	0.69	—	4.92
2012 Aug. 05	11	26.7	2.4	10.1	—	—	3.28
2012 Aug. 10*	**29**	**32.5**	**1.1**	**14.2**	**0.67**	**0.60**	**13.1**
2012 Sept. 08	**10**	**12.2**	**1.2**	**7.8**	**0.78**	—	**0.38**
2012 Sept. 18	14	16.0	1.1	6.9	—	—	1.04
2012 Oct. 06	15	24.1	1.6	4.6	0.75	0.61	24.1
2012 Oct. 14	22	13.2	0.6	2.3	0.79	0.61	9.39
2012 Oct. 19	**14**	**27.4**	**2.0**	**7.4**	**0.67**	**0.66**	**78.1**

*Events in **bold** represent those more likely to produce erosion in the field.

erosion and sediment transport because they had the highest total precipitations and intensities. However, according to the NAPI, the 5th of August event occurred after a dry period that left the unsaturated soil more conducive to infiltration minimizing runoff. In addition, both events in August occurred during the period of maximum vegetative cover, protecting the soils from raindrops and providing resistance to overland flow in rill and interrill; further reducing soil erosion in the fields. With regard to the October event, corn (*Z. mays*) and soy (*G.max*) fields had been harvested, which left areas of the watershed prone to erosion. Most of the other remaining vegetation had withered, further exposing the soil. Combined with the high NAPIs that reflect initially saturated soils, these elements corroborate the much higher values of the peak flow rates at the outlet and reflect the vulnerable watershed conditions during the aforementioned events.

Parameterization

As mentioned, MHYDAS-Erosion is an event-based, distributed model requiring a set of parameter values for each spatial unit. Geometric SU and RS parameters, such as average slope, and soil stability parameters can be obtained from the same spatially distributed information used for generating SUs and RSs (e.g. crops and tillage practices). The model also requires moisture content (θ_i) as an initial condition based on the NAPI for periods of 48 hours and 5 days, as suggested by Heggen (2001) and Ali *et al.* (2010). Table III shows the input parameters required to run MHYDAS-Erosion. Each parameter has a distinct value for each RS and SU. The micro-watershed has a relatively flat topography with a maximum slope of 3.2% around branch 14 near the outlet and in the southern headwater hillslopes.

Note that all parameters evolve during the year as a function of land cover (e.g. growth stage of crops and tillage practices).

Table III. MHYDAS-Erosion parameters

Parameter	Description	Unit
SU		
K_s	Saturated hydraulic conductivity	$m\,s^{-1}$
h_c	Air entry potential	m
θ_r	Soil residual humidity	$m^3\,m^{-3}$
θ_r	Soil saturation moisture	$m^3\,m^{-3}$
n_{SU}	Manning's roughness coefficient	$s\,m^{-1/3}$
A_s	Aggregate stability index	—
N_{rill}	Number of rills/gullies	—
W	Rill/gulley width	m
$d50_{sed}$	Median sediment diameter	m
τ_c	Critical soil shear stress	*Pa*
Transfcode	Interface type indicator (SU-SU or SU-RS)	—
K_r	Rill erodibility	$s\,m^{-1}$
$CETI_{max}$	Maximum transport coef. from interrill erosion	—
Strip.width	Vegetated filter width	m
Strip.Density	Density of vegetation in filter	—
RS		
K_s	Saturated hydraulic conductivity	$m\,s^{-1}$
n_{RS}	Manning's roughness coefficient	$s\,m^{-1/3}$
K_r	Rill erodibility	$s\,m^{-1}$
τ_c	Critical soil shear stress	Pa

Hydrological parameters. The hydrological input parameters include hydraulic conductivity (K_s), air entry potential (h_c), residual and saturated moisture contents (θ_s and θ_r) and Manning's roughness coefficient for SUs and RSs (n_{SU} and n_{RS}). These parameters are mainly linked to the processes that govern the separation of precipitation into surface and sub-surface flows as well as surface flow velocities and heights. Table IV introduces the different values assigned to the SUs and RSs as a function of crop growth or activity in the field. The values chosen for the Manning's coefficient are based on field observations throughout the summer and fall of 2012 and on recommended values (see Albertson and Simons 1964, Chow, 1959).

Table IV. Manning's roughness coefficient values based on each land cover type

Occupation	Manning start/end of season	Manning mature	Manning harvested	Manning plowed
Unknown	0.03	0.035	0.03	0.030
Corn (*Zea mays*)	0.032	0.040	0.032	0.027
Oat (*Avena sativa*)	0.032	0.450	0.032	0.030
Soy (*Glycine max*)	0.030	0.040	0.035	0.027
Prairie	0.040	0.050	0.040	—
Prairie (late growth)	0.030	0.045	0.040	—
Forest	0.100	0.150	—	—
Urban	0.025	0.027	—	—

The residual and saturation moisture values (θ_s and θ_r) are linked to the soil texture available from the aforementioned 2009 soil survey conducted by AAFC (Lamontagne *et al*., 2010), and the values provided by the U.S. Department of Agriculture (see USDA NCRS Rescources, 2014). However, the hydraulic conductivity values are not only strongly influenced by the soil type but also by farming practices such as plowing and other soil tillage practices. Saturated hydraulic conductivity values (K_s) for SUs and RSs were found by intersecting the soil and hydrological unit maps and identifying the dominant soil type for each unit; the values range from 0.1 mm/h to 47 mm/h. The SU K_s values for plowed soils were multiplied by an order of magnitude because *in situ* measurements were not available. Naturally occurring macropores have been found to significantly increase hydraulic conductivity and induce a concentrated flow in densely vegetated areas such as woodlands and unaltered soil (Beven and Germann, 1982). To account for these phenomena, the K_s values assigned to forested soils were an order of magnitude greater than those recorded in the soil surveys.

Finally, the air entry potential values (h_c) are linked to residual and saturation moisture values and topsoil porosity. The air entry potential values varied from 0.20 m to 0.32 m and were allocated by weighing a fixed maximum value (0.35 m) with the topsoil porosity values observed by AAFC (Lamontagne *et al*., 2010).

Erosion and transport parameters. Table V presents all the values of the erosion parameters according to the land cover or soil type. These parameters are specific to soil erosion and sediment transport because they alter soil cohesion, transport and deposition properties. As discussed above, MHYDAS-Erosion simulates these processes in two stages because they are induced by: (i) the impact of raindrops between rills and (ii) the concentrated surface flow within rills; the latter stage is defined as preferential flow that is naturally formed by the topography or tilling practices such as plowing.

Table V. Erosion parameter values of different land cover or soil types

Parameter	Value	Land use or soil type
A_s	0.001	Farm roads
	0.7	Annual crops
	0.5	Prairies and forests
$CETI_{max}$	0.25	Farm roads
	0.06	Annual crops (tilled)
	0.12	Annual crops (tilled)
	0.01	Prairies and forests
τ_c	100	Farm roads
	2	Sand, loamy sands, sandy loams
	3	Loams, silty loams
	10	Clay, loamy clay
K_r	1.00E - 09	Farm roads
	0.1	Sand, loamy sands, sandy loams
	0.01	Loams, silty loams
	0.005	Clay, loamy clay

Processes that affect the detachment and transport by rainfall only occur on SUs and are mainly contained in the areas between rills. The interrill detachment equations rely on the initial values of the soil aggregate stability index between rills (A_s) and the transport efficiency coefficient between rills (*CETI*), where $CETI_{max}$ is the maximum possible value of *CETI*.

Sediment detachment and transport equations of the surface flow within rills (SU level) and within the drainage network (RS level) rely on initial values of rill erodibility (K_r) and critical soil shear stress (τ_c). Values suggested by Gumiere *et al*. (2010) for each parameter are attributed to each SU or RS according to land cover and soil type. The number of rills per SU (N_{rill}) is limited to 30 to ensure the model stability. As all SUs cover an area large enough for more than 30 rills to occur, the maximum number of rills is attributed to most SUs. The rill width (W) is derived according to *in situ* observations and crop type. For example, erosion rills are distributed irregularly and have widths between 10 and 50 cm. Rills

in corn (*Z. mays*) fields are regularly spaced and have widths between 60 and 75 cm.

Model application

Calibration and validation strategy. The model was first calibrated by adjusting the most sensitive input parameters found in the equations that govern infiltration and surface flow. Adjustments were made to the infiltration rates and diffusive wave speeds according to the analytical solutions of the Morel-Seytoux (1978) and Hayami (1951) equations, respectively. Furthermore, sensitivity analyses performed by Cheviron *et al*. (2010) revealed that the most sensitive parameters of MHYDAS-Erosion were K_s, N_{rill}, K_r and A_s. The evaluation metrics used to assess model calibration are introduced in Table VI. They included the Nash–Sutcliffe coefficient (E_{NS}), the root mean squared error (*RMSE*), the coefficient of determination (R^2), the relative volume error (*RVE*) and the percentage error at peak (*PEP*) (Dawson *et al*., 2007).

The initial parameter values defined for the eight rainfall–runoff events observed during the field campaign (summer 2012) provided the datasets for model calibration and validation. However, the growing season during which the data collection campaign occurred was abnormally dry, with 60 mm to 80 mm less rainfall than the average, which not only led to a small number of datasets (i.e. the aforementioned rainfall events), but also low-amplitude and low-intensity events. By comparing the simulated flow rates and sediment fluxes with recorded data and as suggested by Gumiere *et al*. (2010), values of the calibration parameters were first set within realistic ranges with *a priori* spatially distributed information. Initial simulations and calibration attempts showed that for all but one dataset, the resulting water heights in field rills simulated by MHYDAS were below the stability threshold for erosion to occur. Therefore, no calibration events contained rainfall intensities large enough to generate significant erosion and transport within the fields. Considering the small number of datasets and the nature of the available data, a standard calibration and validation exercise was not truly possible. The alternative approach was to verify the validity of the simulated erosion processes. To achieve this, the following three-step procedure was designed: (i) a dataset was selected and simulations that best represented actual, high-magnitude events producing erosion within the fields were run; (ii) a comparison of the simulated sediment loads with those of a neighbouring watershed where data were available for similar events and initial conditions was performed, and (iii) simulations of events with different lengths and intensities were run to test the model for all available initial conditions under a variety of stresses.

Table VI. Metrics and their range used to evaluate the performance of MHYDAS-Erosion

Criteria	Equation	Range
E_{NS}	$E_{NS} = 1 - \frac{\sum_{i=1}^{n}\left(Y_i - \widehat{Y}_i\right)^2}{\sum_{i=1}^{n}\left(Y_i - \overline{Y}\right)^2}$	[-∞, 1]
RMSE	$RMSE = \sqrt{\frac{1}{n}\sum_{i=1}^{n}\left(Y_i - \widehat{Y}_i\right)^2}$	[0, +∞]
R^2	$R^2 = \left[\frac{\sum_{i=1}^{n}\left(Y_i - \overline{Y}\right)\left(\widehat{Y}_i - \widetilde{Y}\right)}{\sqrt{\sum_{i=1}^{n}\left(Y_i - \overline{Y}\right)^2 \sum_{i=1}^{n}\left(\widehat{Y}_i - \widetilde{Y}\right)^2}}\right]^2$	[0, 1]
RVE	$RVE = \frac{\sum_{i=1}^{n}\left(Y_i - \widehat{Y}_i\right)}{\sum_{i=1}^{n} Y_i}$	[-∞,+∞]
PEP	$PEP = \frac{max(Y_i) - max\left(\widehat{Y}_i\right)}{max(Y_i)} \cdot 100$	[-∞, +∞]

Where Y_i is the observed value, $\hat{Y}_i$ is the simulated value, n is the number of elements in the sample and $\overline{Y}$ and $\widetilde{Y}$ are the average observed and simulated values, respectively

We chose the dataset of the 19th of October for step (i) because it represented the initial conditions that were most likely to generate soil erosion. It had the greatest amount of recently plowed cropland and little-to-no vegetation cover. This recorded event also had the highest flow rates, which further represents precipitation events with low recurrences.

For step (ii), the simulated sediment fluxes for the 19th of October were compared with those of the Lennoxville watershed where the sediment fluxes for similar precipitation events are available. The latter watershed, studied by Duchemin *et al*. (2001), is an intensively farmed, 0.78-km^2, area located 150 km southwest of the study site. This watershed has geomorphological characteristics that are comparable to those of the watershed in the present study. It is divided by two distinct sub-watersheds that are drained by separate branches that converge near the watershed outlet. It also has similar slopes, land cover and reach lengths.

For step (iii), simulations were run using a variety of synthetic design rainfalls with return periods of 10, 50 and 100 years to form a total of 18 simulations. The total precipitation for each return period corresponded to the intensity–duration–frequency (IDF) curves provided by the nearest Environment Canada weather station, that of Lévis (a few kilometres away), with available curves (cfclimate.weather.gc.ca/prods_servs/engineering_e.html). Although these curves are conservative in terms of maximum intensity, their common use in hydraulic design allows for the micro-watershed to be studied under high hydrologic stress within well-known conditions. Synthetic rainfalls were chosen as opposed to actual

Table VII. Study rainfalls along with values of total precipitation and maximum intensity as a function of return period

Simulation	Precipitation (mm)	Maximum intensity ($mm\,h^{-1}$)
Chicago 6 h	55.6	29.8
10 years	71.4	38.2
50 years	78.1	41.8
Chicago 24 h		
10 years	75.0	26.6
50 years	92.5	32.8
100 years	99.9	35.5
Triangular 24 h		
10 years	75.0	5.8
50 years	92.5	7.1
100 years	99.9	7.7
Irene	166.2	31.5

events because they offer greater control over the chosen intensities, temporal distribution and resolution. The 24-h triangular distribution is most representative of rainfall events observed in the province of Quebec (Pelletier *et al.*, 2009). The 6-h and 24-h Chicago rainfall distributions have very high rainfall intensities that result in potentially high erosion rates. An additional simulation was run using an actual high-intensity precipitation event recorded during the passage of the tail-end of Hurricane Irene in 2011. This event is known to have caused unprecedented soil erosion and flooding in the study region. The recorded rainfall was 166 mm over 16 h, classifying the event at a recurrence rate greater than 100 years. Table VII shows the distributions and total precipitation based on their return periods.

Simulation of vegetative filter strips. Two scenarios were considered for the spatial configuration of vegetated filter strips.

- 5-m wide vegetated filter strips placed at the downstream end of every SU connection.
- Vegetated filter strips placed at the downstream end of the most vulnerable SUs.

For the first scenario, we assumed that each topological connection contains a 5-m vegetated filter strip, corresponding to a minimum width for areas with moderate erosion rates (e.g. Muscutt *et al.*, 1993). This is the equivalent of placing vegetated filter strips on both banks of each RS and at the topological connections between the SUs within the same fields where there is a change in the hydrological properties.

RESULTS AND DISCUSSION

Model calibration and validation

A sample result of the hydrological calibration of the model is shown in Figure 6, that for the 19th of October, that step (i). The model was observed to simulate flow rates fairly well at the watershed outlet with overall satisfying performances (R^2: 0.727 and E_{NS}: 0.726) and very similar peak flows with good reproduction for the total volume (*PEP*: 5.62% and *RVE*: −0.05). The distinct bimodal nature of the hydrograph was observed in all the other simulations and is likely associated with the different response times of each branch (branches 14 and 15).

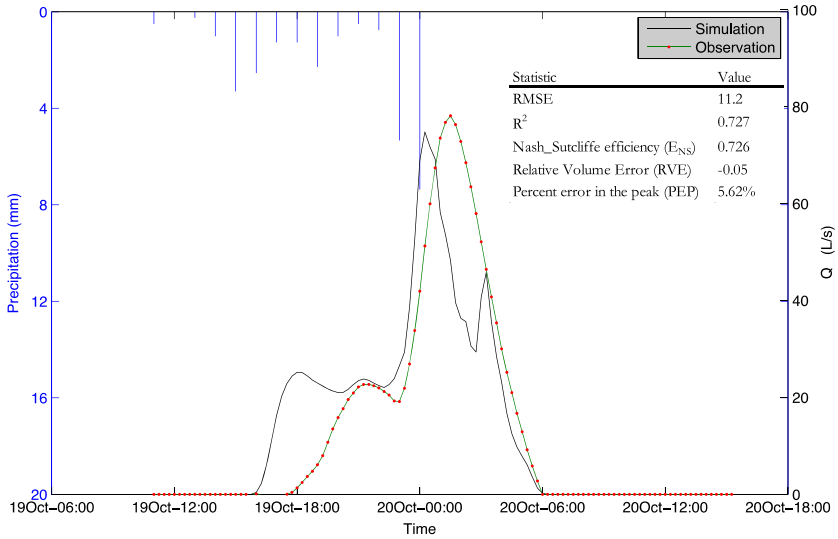

Figure 6. Calibration results of the outlet discharge for the 19th of October 2012

Table VIII. Comparison between Lennoxville and Bras d'Henri micro-watersheds

Comparable feature	Bras d'Henri	Lennoxville
Area	2.4 km^2	0.78 km^2
Mean slope	2.5 ± 1.2%	6.6%
Cropland and prairie cover	85% (61% and 24%)	92% (33% and 59%)
Maximum reach length to the outlet	1.7 km	1.0 km
Total precipitation per event	55 to 99 mm	43 to 57 mm
Sediment export at the outlet	17 to 96 kg/ha	50 to 71 kg/ha

For step (ii), the recorded precipitation events at the Lennoxville watershed (ranging from 43 to 57 mm) produced sediment loads at the outlet of 50 to 71 kg/ha. The simulated precipitation events at Bras d'Henri, which ranged from 55 to 99 mm, were in the same order of magnitude with sediment loads at the outlet of 17 to 97 kg/ha (see Table VIII).

Results for step (iii) are introduced in Figures 7 and 8. Figure 7 shows the simulated hydrographs at the watershed outlet using the Irene (a), 100-year 24-h Chicago (b) and Triangular (c) precipitation data. Figures 8a, 8b and 8c show the corresponding erosion maps. The other maps of Figure 8 will be discussed later. For all three events, the SUs with low slopes (<1%) and woodland consistently yielded low to no sediment, and the SUs with greater slopes and recently plowed fields had much higher sediment yields, as expected. Overall, the SU soil loss varied between 0 and 29.7 T/ha.

The precipitation from Irene (a), which was the largest event simulated in terms of volume (166 mm over 16 h), showed high sediment fluxes at SU outlets throughout the watershed; 37% of the total area had SU sediment exports of more than 0.2 T/ha, while 11% of the area had SU sediment exports between 8.0 and 30 T/ha (as seen in Table IX). The highest SU sediment exports (in proportion to the area) were identified in tilled soy (*G. max*) fields and prairies at the outer edges of the watershed where the slopes were greater (3%+). The total sediment fluxes at the outlet of the entire watershed was 374 kg/ha.

The 100-year Chicago event (b) had the largest synthetic precipitation and high sediment fluxes from all SUs. However, compared with Irene, the simulations showed a larger proportion of SUs (48%) with cumulative sediment exports larger than 0.2 T/ha and a much lower proportion of SUs (2.5%) with sediment exports between 8.0 and 30 T/ha. As observed in Figure 7b, the Chicago rainfall behaves as a pulse event that quickly leads to maximum infiltration throughout the watershed and generates higher Hortonian flow heights in rills, which explains the larger proportion of SUs with sediment exports larger than 0.2 T/ha. However, because Irene developed more gradually, as observed in Figure 7a (with a sustained but less intense pulse than the Chicago event), the overall larger volume of rain caused greater infiltration throughout the event. Thus, SUs prone to erosion delivered considerably more sediments during the event and represented a larger proportion of the watershed area at 8.0 to 30 T/ha. These results corresponded to much smaller overall total sediment flux at the watershed outlet, that is 112 kg/ha.

The Triangular event (Figures 7 and 8c) has a total precipitation equivalent to the Chicago event, but produced considerably less sediment transport throughout the watershed because it develops very gradually over time; only 1.9% of the total SU area exported more than 0.005 T/ha. Again, SUs that did export sediments were

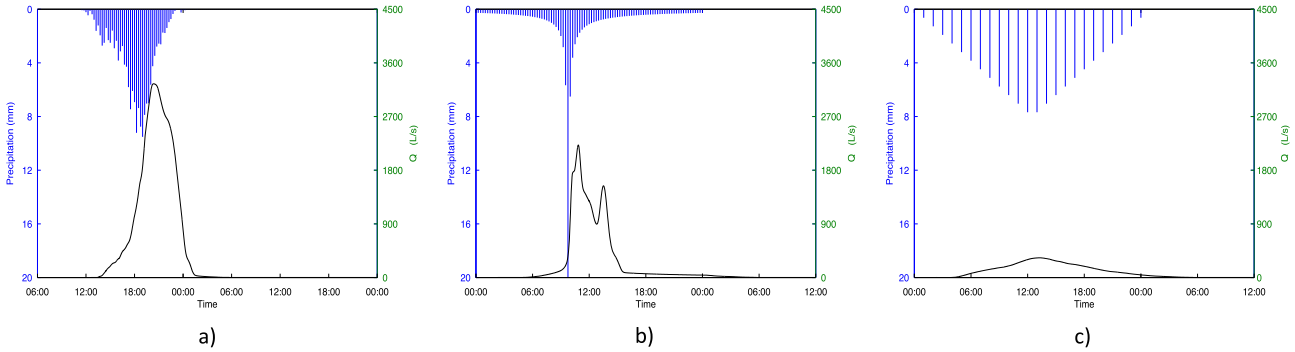

Figure 7. Simulated hydrographs at the watershed outlet using the 19th of October dataset and precipitation from Irene (a), the 100-year 24-h Chicago event (b) and the Triangular event (c)

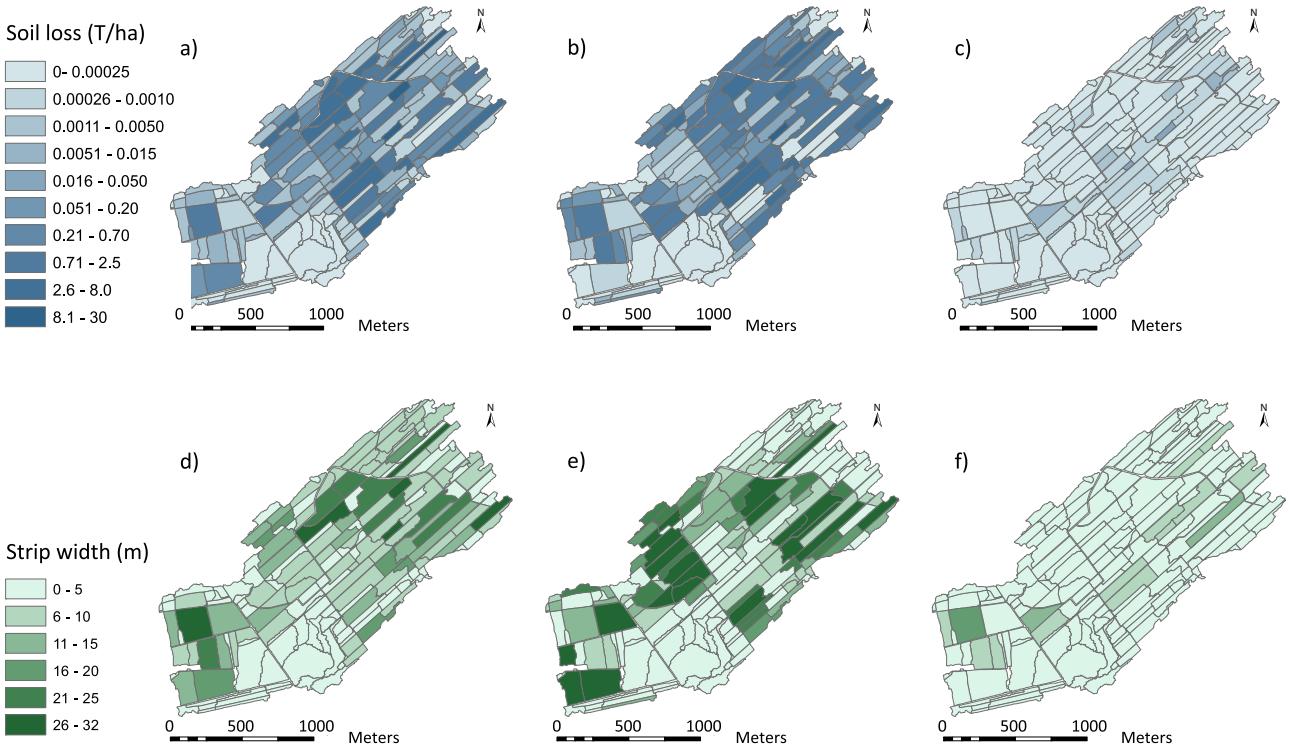

Figure 8. MHYDHAS-Erosion (top row) and associated VFDM (bottom row) simulations using the 19th of October dataset and precipitation from Irene (a and d), the 100-year 24-h Chicago event (b and e) and the Triangular event (c and f). The erosion figures show the relative soil loss per SU for each event, and the associated VFDM figures show the required vegetated filter strip width at the downstream end of each SU to capture 60% of the sediment

Table IX. Cumulative SU area per sediment flux for simulations using the 19th of October dataset and precipitation from Irene, the 100-year 24-h Chicago event and the Triangular event

Soil flux range in SUs T/ha	Irene	Chicago 24 h 100 years	Triangular 24 h 100 years
0.00025 +	83%	80%	30%
0.001 +	77%	76%	6.5%
0.005 +	55%	60%	1.9%
0.02 +	46%	57%	—
0.05 +	43%	54%	—
0.2 +	37%	48%	—
0.7 +	30%	39%	—
2.5 +	18%	22%	—
8.0 – 30	11%	2.5%	—

mostly in soy (*G. max*) fields. However, sediment flux at the outlet was still at 19 T/ha for the event.

Comparing sediment fluxes for RSs with those for SUs, it was found that throughout all the simulations driven by triangular events, 58.6 ± 2.8 times more sediments at the outlet came from RS erosion and transport processes (16 ± 2.8 kg ha^{-1} from RSs/0.27 ± 0.12 kg ha^{-1} from SUs). Conversely, for Chicago simulations, it was found that 7.5 ± 0.5 times more sediments at the outlet came from cropland SUs (550 ± 190 kg ha^{-1} from SUs/72 ± 23 kg ha^{-1} from RSs). Thus, the infiltration process induced by events with intensities similar to those of the triangular rainfall correlated with precipitation; the flow in rills being too low for transport and erosion processes in fields. However, sediment fluxes at the outlet amounted to 22 kg/ha for agricultural land, which demonstrates that runoff in SUs still accumulates in the RS network inducing transport and erosion in the drainage network.

Because the validation procedure for the model suggests that adequate estimates could be obtained, estimating the errors of predicted sediment fluxes at the SU level and at the watershed outlet was deemed beyond the scope of this study. However, the 19th of October rainfall closely resembled the triangular rainfall, albeit with less total

accumulation. This similarity suggests that simulations for triangular rainfall events corroborated fairly well with the actual watershed behaviour. Conversely, simulations for events such as Irene most likely overestimated soil loss and sediment transport because results were beyond the domain of model functions given the calibrated initial conditions. Nevertheless, further verifications were conducted by comparing Irene-simulated SU sediment fluxes with event-based sub-watershed-scale simulations for a Mediterranean vineyard reported by Casasnovas *et al.* (2002) and with recorded sub-watershed soil loss values in similar environments reported by Ramos and Porta (1997). For these studies, precipitation values ranged from 127 mm to 215 mm and induced 22 T/ha of soil losses (erosion within rills only) to 207 T/ha (entire sub-watershed). Considering that Irene's precipitation is similar to typical Mediterranean rainfall, it can be said that the MHYDAS-Erosion simulated values have reasonable magnitudes.

Simulations of vegetated filter strips

The simulations using Irene's precipitation suggest that placing 5-m strips at the downstream end of each SU could reduce the total SU sediment export to the drainage network by $52\% \pm 0.90\%$ ($524\,kg\,ha^{-1}$ out of $1015\,kg\,ha^{-1}$). Better abatement performances may be expected for events with smaller return periods than those of Irene because the flow heights in SU rills and gullies would be smaller.

Figure 8 shows the predicted buffer strip width required at the downstream end of all SUs to capture, on average, 60% of the incoming sediment passing through for Irene (d), the 100-year 24-h Chicago storm (e) and the triangular synthetic storm (f). SUs with consistently high soil losses throughout all simulations need wide vegetated filters to capture 60% of the incoming sediment. This requirement is specifically apparent in (f). Again, Irene (d) reveals fewer SUs that require large strips than those for the Chicago event because a higher Hortonian flow is produced by the latter, sustained high-intensity pulse.

The second scenario consisted of placing vegetated filter strips at the downstream end of SUs sensitive to erosion (e.g. the soy (*G. max*) fields discussed above) throughout all simulations that run during the model validation process. The results show that for the Irene event, placing 20-m to 30-m wide vegetated filter strips at the downstream end of the most problematic SUs (essentially converting these SUs to high grasses, which comprise 4% of the watershed area) could reduce the global SU sediment export to the drainage network by $31\% \pm 6.8\%$ ($310\,kg\,ha^{-1}$ out of $1015\,kg\,ha^{-1}$). These values are representative of uniform flow conditions through vegetative filter strips as modelled by VFDM. As preferential flows occur naturally, the filter's ability to slow down the flow is potentially overestimated albeit unknown. The latter phenomenon is the subject of current modeling development.

It is noteworthy the extensive litterateur review conducted by Gumiere *et al.* (2011) reported that field studies showed that vegetated filter strips can have high sediment trapping efficiencies, exceeding 50% for the total sediment load. Furthermore, Nigel *et al.* (2014) showed using high-resolution, remote sensing, raster-based information showed that for a intensively farmed 108-km^2 watershed of in Québec, that an extended riparian buffer strip concept would enable reducing soil erosion in riverine areas from 361 to $1.0\,t\,year^{-1}$ (1.9 to $0.005\,t\,ha^{-1}\,year^{-1}$), thereby reducing soil erosion at the watershed scale by 40% (calculated with the Revised Universal Soil Loss Equation, RUSLE). The extended riparian buffer strip concept would require the conversion of 7% of the $29\,km^2$ of agricultural land. Therefore, these reported values illustrate the sediment abatement rates reported herein are in all likelihood reasonable.

CONCLUSION

This paper introduced the first application of MHYDAS-Erosion to a study site under a temperate climate. The study enabled an evaluation of the impact of vegetated filter strips on the sedimentological connectivity of a 2.5-km^2 watershed in southern Quebec, Canada. A discretization method for MHYDAS-Erosion was developed using PHYSITEL and provided an accurate representation of the agricultural watershed. The discretization was further refined with *in situ* observations, in order to account for small-scale flow discontinuities generated by BMPs. The simulations produced sediment fluxes of the correct order of magnitude at the watershed outlet by comparing a variety of fluxes induced by synthetically designed precipitation events with those available from a similar watershed under similar rainfall conditions. The surrogate calibration and validation exercise implies that simulated sediment fluxes are first-approximation estimates, and further validation should be conducted to assess the sedimentological dynamics of the study watershed.

Because the model is spatially distributed, it is possible to visualize erosion rates at different locations within the watershed. The simulations show that for high-intensity events, the majority of the erosion occurs in fields because precipitation rates exceed maximum infiltration rates; thus, Hortonian flow in rills developing in cropland SUs contribute 7.5 ± 0.5 times more sediments at the outlet than do RSs (i.e. the drainage network). On the other end, simulations for lower-intensity events show that most of the erosion occurs in the drainage network,

with 58.6 ± 2.8 times more sediments at the outlet originating from RSs because flow heights in RSs are high enough for erosion and transport processes to occur.

Simulations of an Irene-type precipitation event show that placing 5-m strips at the downstream end of each SU reduces the sediment output from the fields by 52% ± 0.90%. Placing 20-m to 30-m wide vegetated filter strips at the downstream end of the most problematic SUs (i.e. converting 4% of the total cropland cover to high grasses) could reduce the global SU sediment export to the drainage network by 31% ± 6.8%. These results are of interest for watershed decision makers because abatement efficiency is expected to be higher for events with shorter return periods than that of Irene, which is greater than 100 years.

Local relief can cause highly concentrated flows that form gullies within vegetated filter strips. Because the model does not simulate concentrated flow through vegetated filter strips, the simulated abatements were probably overestimated. Undergoing efforts focus on fully coupling VFDM and MHYDAS-Erosion so that abatement effects are carried over from one time step to another during the simulations. Including a diffusive flow module within VFDM, such as the interrill flow modelled by MHYDAS-Erosion, would also improve the representation of vegetated filter strip abatement efficiencies. As shown by Gumiere *et al.* (2014), the proposed modeling framework is well suited for exploring different BMP location strategies.

ACKNOWLEDGEMENTS

The authors wish to thank Catherine Bossé, Geneviève Montminy, Michel Nolin, Luc Lamontagne and Mario Deschênes of Agriculture and Agri-Food Canada (AAFC) for providing data. Special thanks to Brook Harker and David Kiely of AAFC for their coordination of the WEBs (Watershed Evaluation of Beneficial Management Practices) project. Additional thanks are given to Isabelle Beaudin and Aubert Micheaud (IRDA) for providing a detailed DEM for the watershed. This project received financial support from AAFC (A. N. Rousseau, principal investigator of the project 'Hydrological and Economic Modelling of the Impact of Beneficial Managements Practices on Water Quality in an Agricultural Watershed' as part of the Growing Forward WEBs research and development program).

REFERENCES

AAFC Agriculture and Agroalimentaire Canada. (2013). Données tirées de l'atlas géographique du projet du Bras d'Henri/Fourchette, Québec (2004–2013) dans le cadre du programme national d'Évaluation des Pratiques de gestion bénéfiques à l'échelle des bassins hydrographiques (ÉPBH). Centre de recherche et de développement sur les sols et les grandes cultures, Sainte-Foy, Québec, Canada.

Akram S, Yu B, Ghadiri H. 2015. Modelling flow and sediment trapping upstream and within grass buffer strips. *Hydrological Processes* **29**: 3179–3192.

Albertson ML, Simons DB. 1964. Fluid mechanics. In *Handbook of Applied Hydrology*. Chow VT (ed). McGraw-Hill: New York; **7**: 1–49.

Ali S, Ghosh NC, Singh R. 2010. Rainfall–runoff simulation using a normalized antecedent precipitation index. *Hydrological Sciences Journal* **55**(2): 266–274.

Ascough J, Baffaut C, Nearing MA, Liu BY. 1997. The WEPP watershed model: I. Hydrology and erosion. *Transactions of the ASABE* **40**: 921–933.

Bennett JP. 1974. Concepts of mathematical modeling of sediment yield. *Water Resources Research* **10**(3): 485–492.

Beven K, Germann P. 1982. Macropores and water flow in soils. *Water Resources Research* **18**(5): 1311–1325.

Bracken LJ, Croke J. 2007. The concept of hydrological connectivity and its contribution to understanding runoff-dominated geomorphic systems. *Hydrological Processes* **21**(13): 1749–1763.

Callow JN, Smettem KRJ. 2009. The effect of farm dams and constructed banks on hydrologic connectivity and runoff estimation in agricultural landscapes. *Environmental Modelling & Software* **24**(8): 959–968.

Casasnovas JA, Ramos M, Ribes-Dasi M. 2002. Soil erosion caused by extreme rainfall events: mapping and quantification in agricultural plots from very detailed digital elevation models. *Geoderma* **105**(1–2): 125–140.

Cheviron B, Gumiere SJ, Le Bissonnais Y, Moussa R, Raclot D. 2010. Sensitivity analysis of distributed erosion models: Framework. *Water Resources Research* **46**(8: W08508): . DOI:10.1029/2009WR007950.

Chow VT. 1959. *Open channel hydraulics*. McGraw-Hill: New York; 700.

Courant R, Friedrichs K, Lewy H. 1928. On the partial difference equations of mathematical physics. *Mathematische Annalen* **100**(1): 32–74.

Dawson CW, Abrahart RJ, See LM. 2007. HydroTest: a web-based toolbox of evaluation metrics for the standardised assessment of hydrological forecasts. *Environmental Modelling & Software* **22**(7): 1034–1052.

Deletic A. 2005. Sediment transport in urban runoff over grassed areas. *Journal of Hydrology* **301**(1–4): 108–122.

Deletic A, Fletcher TD. 2006. Performance of grass filters used for stormwater treatment—a field and modelling study. *Journal of Hydrology* **317**(3): 261–275.

De Roo APJ, Wesseling CG, Ritsema CJ. 1996. LISEM: a single-event physically based hydrological and soil erosion model for drainage basins. I: theory, input and output. *Hydrological Processes* **10**(8): 1107–1117.

Duchemin M, Lachance M, Morin G, Lagacé R. 2001. Approche géomatique pour simuler l'érosion hydrique et le transport des sédiments à l'échelle des petits bassins versants agricoles. *Water Quality Research Journal of Canada* **36**(3): 435–473.

Finkner S, Nearing M, Foster G, Gilley JE. 1989. A Simplified Equation for Modeling Sediment Transport Capacity. *Transactions of the ASAE* **32**(5): 1587–1593.

Foster GR. 1982. Modelling the erosion process. In *Hydrologic modelling of small watersheds*. Haan CT, Johnson HP, Brakensiek DL (eds). ASAE Monograph No. 5, American Soc. Of Agric. Engr.: St Joseph, Ichigan; 295–380.

Foster GR, Flanagan DC, Nearing MA, Lane LJ, Risse LM, Finkner SC. 1995. Water Erosion Prediction Project (WEPP): technical documentation. Tech. rep. NSERL Report 10. National Soil Erosion Research Laboratory. USDA-ARS-MWA.1196 Soil Building: West Lafayette, IN 47907 – 1196.

Gumiere S, Raclot D, Cheviron B. 2010. MHYDAS-Erosion: a distributed single-storm water erosion model for agricultural catchments. *Hydrological Processes* **25**(11): 1717–1728.

Gumiere SJ, Le Bissonnais Y, Raclot D, Cheviron B. 2011. Vegetated filter effects on sedimentological connectivity of agricultural catchments in erosion modelling: a review. *Earth Surface Processes and Landforms* **36**(1): 3–19.

Gumiere SJ, Rousseau AN, Hallema DW, Isabelle P-E. 2013. Development of VFDM: a riparian vegetated filter dimensioning model for agricultural watersheds. *Canadian Water Resources Journal* **38**(3): 169–184.

Gumiere SJ, Bally JS, Cheviron B, Raclot D, Le Bissonnais Y, Rousseau AN. 2014. Evaluating the impact of the spatial distribution of land management practices on water erosion: a case study of a Mediterranean catchment. *Journal of Hydrologic Engineering* . DOI:10.1061/(ASCE)HE.1943-5584.0001076.

Gumiere SJ, Rousseau AN, Hallema DW, Isabelle P-É. 2015. Corrigendum. *Canadian Water Resources Journal* **40**(2): 235–235. DOI:10.1080/07011784.2015.1017537.

Hayami S. 1951. On the propagation of flood waves. *Bulletins – Disaster Prevention Research Institute, Kyoto University* **1**: 1–16.

Heggen RJ. 2001. Normalized antecedent precipitation index. *Journal of Hydrologic Engineering* **6**: 377–381.

Jetten V, de Roo A, Favis-Mortlock D. 1999. Evaluation of field-scale and catchment-scale soil erosion models. *CATENA* **37**(3): 521–541.

Jetten V, Govers G, Hessel R. 2003. Erosion models: quality of spatial predictions. *Hydrological Processes* **17**(5): 887–900.

Kinnell PIA. 2005. Raindrop-impact-induced erosion processes and prediction: a review. *Hydrological Processes* **19**: 2815–2844.

Knisel, W. 1980. CREAMS: a field-scale model for chemicals, runoff and erosion from agricultural management systems. *USDA Conservation Research Report n.27*. [Available at: http://www.cabdirect.org/abstracts/19801956438.html].

Lagacherie P, Rabotin M, Colin F, Moussa R, Voltz M. 2010. Geo-MHYDAS: a landscape discretization tool for distributed hydrological modeling of cultivated areas. *Computers & Geosciences* **36**(8): 1021–1032.

Lamontagne, L, Martin, A, Nolin, MC. 2010. Étude pédologique du bassin versant du Bras d'Henri (Québec), Laboratoires de pédologie et d'agriculture de précision, Centre de recherche et de développement sur les sols et les grandes cultures, Direction générale de la recherche, Agriculture et Agroalimentaire Canada. Québec (Québec).

Morel-Seytoux HJ. 1978. Derivation of equations for variable rainfall infiltration. *Water Resources Research* **14**(4): 561–568.

Morgan R, Quinton J. 1998. The European Soil Erosion Model (EUROSEM): a dynamic approach for predicting sediment transport from fields and small catchments. *Earth Surface Processes and Landforms* **23**(1): 527–455.

Moussa R. 1996. Analytical Hayami solution for the diffusive wave flood routing problem with lateral inflow. *Hydrological Processes* **10**(9): 1209–1227.

Moussa R, Voltz M, Andrieux P. 2002. Effects of the spatial organization of agricultural management on the hydrological behaviour of a farmed catchment during flood events. *Hydrological Processes* **16**(2): 393–412.

Munoz-Carpena R, Parsons JE, Gilliam JW. 1999. Modeling hydrology and sediment transport in vegetative filter strips. *Journal of Hydrology* **214**(1–4): 111–129.

Muscutt AD, Harris GL, Bailey SW, Davies DB. 1993. Buffer zones to improve water quality: a review of their potential use in UK agriculture. *Agriculture, Ecosystems and Environment* **45**: 59–77.

Neitsch, SL, Arnold, JG, Kiniry, JR, Williams, JR. 2011. Soil and water assessment tool theoretical documentation version 2009. Texas Water Resources Institute. Available at http://repository.tamu.edu/handle/1969.1/128050.

Nigel R, Chokmani K, Novoa J, Rousseau AN, El Alem A. 2014. An extended riparian buffer strip concept for soil conservation and stream protection in agricultural riverine areas. *Canadian Water Resources Journal* **39**(3): 285–301. DOI:10.1080/07011784.2014.942572.

Pelletier G, Anctil F, Filion M. 2009. Characterization of 1-h rainfall temporal patterns using a Kohonen neural network: a Quebec City case study. *Canadian Journal of Civil Engineering* **36**(6): 980–990.

Quilbé R, Rousseau A, Moquet J-S, Savary S, Ricard S, Garbouj MS. 2008. Hydrological responses of a watershed to historical land use evolution and future land use scenarios under climate change conditions. *Hydrology and Earth System Sciences* **12**(1): 101–110.

Ramos MC, Porta J. 1997. Analysis of design criteria for vineyard terraces in the mediterranean area of North East Spain. *Soil Technology* **10**(2): 155–166.

Rousseau A, Dickinson WT, Rudra RP. 1987. Evaluation of best management practices to control phosphorus nonpoint source pollution. *Canadian Agricultural Engineering* **29**(2): 163–168.

Rousseau A, Dickinson WT, Rudra RP, Wall GJ. 1988. A phosphorus transport model for small agricultural watersheds. *Canadian Agricultural Engineering* **30**(2): 213–220.

Rousseau AN, Mailhot A, Quilbé R, Villeneuve J-P. 2005. Information technologies in the wider perspective: integrating management functions across the urban-rural interface. *Environmental Modelling & Software* **20**: 443–455.

Rousseau AN, Fortin J-P, Turcotte R, Royer A, Savary S, Quévy F, Noël P, Paniconi C. 2011. PHYSITEL, a specialized GIS for supporting the implementation of distributed hydrological models. *Water News – Official Magazine of the Canadian Water Resources Association* **31**(1): 18–20.

Rousseau AN, Savary S, Hallema DW, Gumiere SJ, Foulon É. 2013. Modeling the effects of agricultural BMPs on sediments, nutrients, and water quality of the Beaurivage River watershed (Quebec, Canada). *Canadian Water Resources Journal* **38**(2): 99–120.

Shi Z-H, Yan F-L, Li L, Li Z-X, Cai C-F. 2010. Interrill erosion from disturbed and undisturbed samples in relation to topsoil aggregate stability in red soils from subtropical China. *CATENA* **81**(3): 240–248.

Soulsby RL. 1997. *Dynamics of marine sands: a manual for practical applications*. Thomas Telford: London.

USDA NCRS Rescources. 2014. <http://goo.gl/9MXxEb> accessed 3rd Febuary 2014.

Woolhiser, D-A, Smith, R-E, Goodrich, D-C, 1990. KINEROS, a kinematic runoff and erosion model: documentation and user manual. *U.S. Department of Agriculture*, *Agricultural Research Service*, p. 130.

Yan F-L, Shi Z-H, Li Z-X, Cai C-F. 2008. Estimating interrill soil erosion from aggregate stability of Ultisols in subtropical China. *Soil and Tillage Research* **100**(1): 34–41.

Young R, Onstad C. 1989. AGNPS: a nonpoint-source pollution model for evaluating agricultural watersheds. *Journal of Soil and Water Conservation* **44**(2): 168–173.

Zhang B, Horn R. 2001. Mechanisms of aggregate stabilization in Ultisols from subtropical China. *Geoderma* **99**: 123–145.

